TU/e EINDHOVEN UNIVERSITY OF TECHNOLOGY

Age-related changes in bone strength from HR-pQCT derived microarchitectural parameters with an emphasis on the role of cortical porosity

Citation for published version (APA):
Vilayphiou, N., Boutroy, S., Sornay-Rendu, E., Van Rietbergen, B., & Chapurlat, R. (2016). Age-related changes in bone strength from HR-pQCT derived microarchitectural parameters with an emphasis on the role of cortical porosity. *Bone*, *83*, 233-240. https://doi.org/10.1016/j.bone.2015.10.012

Document license:
Unspecified

DOI:
10.1016/j.bone.2015.10.012

Document status and date:
Published: 01/02/2016

Document Version:
Accepted manuscript including changes made at the peer-review stage

Please check the document version of this publication:

• A submitted manuscript is the version of the article upon submission and before peer-review. There can be important differences between the submitted version and the official published version of record. People interested in the research are advised to contact the author for the final version of the publication, or visit the DOI to the publisher's website.
• The final author version and the galley proof are versions of the publication after peer review.
• The final published version features the final layout of the paper including the volume, issue and page numbers.

Link to publication

General rights
Copyright and moral rights for the publications made accessible in the public portal are retained by the authors and/or other copyright owners and it is a condition of accessing publications that users recognise and abide by the legal requirements associated with these rights.

• Users may download and print one copy of any publication from the public portal for the purpose of private study or research.
• You may not further distribute the material or use it for any profit-making activity or commercial gain
• You may freely distribute the URL identifying the publication in the public portal.

If the publication is distributed under the terms of Article 25fa of the Dutch Copyright Act, indicated by the “Taverne” license above, please follow below link for the End User Agreement:

www.tue.nl/taverne

Take down policy
If you believe that this document breaches copyright please contact us at:

openaccess@tue.nl

providing details and we will investigate your claim.

Download date: 16. Nov. 2023

Age-related changes in bone strength from HR-pQCT derived microarchitectural parameters with an emphasis on the role of cortical porosity

Nicolas VILAYPHIOU[1,2], Stephanie BOUTROY[1], Elisabeth SORNAY-RENDU[1], Bert VAN RIETBERGEN[3], and Roland CHAPURLAT[1]

[1]INSERM Research Unit 1033 and Université de Lyon, Lyon, France.
[2]Scanco Medical AG, Bruttisellen, Switzerland
[3]Department of Biomedical Engineering, Eindhoven University of Technology, Eindhoven, The Netherlands.

nvilayphiou@scanco.ch
stephanie.boutroy@inserm.fr
elisabeth.rendu@inserm.fr
B.v.Rietbergen@tue.nl
roland.chapurlat@inserm.fr

Running title: of bone strength and cortical porosity

This study was supported in part by the ECTS/Servier Fellowship grant.

Number of words:
Number of figures and tables: 6

Author contact information and person to whom reprint requests should be addressed:
Pr Roland CHAPURLAT, INSERM Unit 1033, Hôpital Edouard Herriot, Pavillon F, 69437 Lyon Cedex 03, France. Tel: +33 472 11 74 84. Fax: +33 472 11 74 83. e-mail: roland.charpulat@inserm.fr

Dr Vilayphiou is now an employee of Scanco Medical AG.
Dr van Rietbergen serves as consultant for Scanco Medical AG.
All other authors have no conflict of interest.

ABSTRACT

The high resolution peripheral computed tomography (HR-pQCT) technique has seen recent developments with regard to the assessment of cortical porosity. In this study, we investigated the role of cortical porosity on bone strength in a large cohort of women.

The distal radius and distal tibia were scanned by HR-pQCT. We assessed bone strength by estimating the failure load by microfinite element analysis (μFEA), with isotropic and homogeneous material properties. We built a multivariate model to predict it, using a few microarchitecture variables including cortical porosity to predict the failure load.

Among 857 Caucasian women analyzed with μFEA, we found that cortical and trabecular properties, along with the failure load, impaired slightly with advancing age in premenopausal women, the correlations with age being modest, with $|r_{age}|$ ranging from 0.14 to 0.38. After the onset of the menopause, those relationships with age were stronger for most parameters at both sites, with $|r_{age}|$ ranging from 0.10 to 0.64, notably for cortical porosity and failure load, which were markedly deteriorated with increasing age. Our multivariate model using microarchitecture parameters revealed that cortical porosity played a significant role in bone strength prediction, with semipartial r^2=0.22 but only at the tibia for postmenopausal women.

In conclusion, in our large cohort of women, we observed a small decline of bone strength at the tibia before the onset of menopause. We also found an increase of cortical porosity at both scanned sites in premenopausal women. Moreover, in postmenopausal women, the relatively high increase of cortical porosity accounted for the decline in bone strength only at the tibia.

Keywords: high resolution peripheral quantitative computed tomography, finite element analysis, osteoporosis, microarchitecture, cortical porosity.

Highlights

- In this work, we analyzed the contribution of cortical porosity in the prediction of bone strength determined by μFEA at the distal radius and tibia, scanned by HR-pQCT
- The study is performed on the complete OFELY cohort, using data from the first visit where HR-pQCT exams could be done.
- Cortical porosity showed an exponential increase with age at both the distal radius and tibia when bone failure load decreased with age following a quadratic law.
- Cortical porosity seemed to have sizeable effects compared to other parameters, only at the distal tibia in postmenopausal women.

INTRODUCTION

The current standard for osteoporosis diagnosis is the measurement of areal bone mineral density (aBMD) by Dual X-ray Absorptiometry (DXA), but its sensitivity and specificity are still inadequate for the prediction of fragility fractures in postmenopausal women (1, 2). Indeed, this assessment of bone mass only partially explains bone strength, and many fractures occur in women with a T-score above the WHO definition of osteoporosis (3, 4). Recent developments of quantitative computed tomography (QCT) and finite element (FE) modelling techniques opened the path for investigating bone fragility using a mechanical rather than a densitometric approach. Based on such analysis, it is possible to estimate bone strength and to compare it directly to estimates of the loads that occur during a fall (5).

There is growing interest in studying changes in trabecular bone strength and microarchitecture. Several studies have reported independent associations of microarchitectural features with prevalent fragility fractures (6-12). Nevertheless, in most studies the associated value of such microstructural parameters, or combinations thereof, with bone fracture risk is not much better than that of areal bone mineral density. A possible explanation for this is that total bone strength is also largely determined by the integrity of cortical bone which, in most of these studies, is quantified only by its thickness.

High resolution peripheral QCT (HR-pQCT) enables the acquisition of detailed features of cortical and trabecular bone. Since the development of a morphometric method to enhance the semi-automatic detection of the endosteal limit of cortical bone, cortical porosity assessment has been added to microstructural features accessible with HR-pQCT (13-15).

MacDonald et. al showed in a population based study a second order relationship from 20 to 98 years old between cortical porosity and age, with increases in porosity ranging from 6 to 16% and from 9 to 28% at the distal radius and tibia, respectively (16).

There is a growing body of evidence for the contribution of cortical porosity to bone fragility (17) (14, 16, 18-21). In *in-vitro* studies, an increase of only 4% in cortical porosity can increase the crack propagation by 84% (18). It was also reported that an increase of up to 10% in porosity reduced by

two-fold the maximum stress the bone could sustain before fracture (19). The value of cortical porosity to predict incident fracture, however, remains to be established.

Although it is clear that increased cortical porosity with aging is associated with reduced bone strength, it is yet unclear what its actual contribution is. Obviously, the trabecular bone strength is also decreased with aging, such that at least part of the bone strength loss will be due to changes in the cancellous compartment. The distal ends of the peripheral skeleton typically assessed by HR-pQCT scanning present a thin cortical shell with very high gradient of thickness along the longitudinal axis, at the radius particularly, the cortical thickness can vary from 0.2 to 1.2 mm from one end of the scanned region to the other (22). A large increase in cortical porosity in such a thin material challenges our understanding of its interaction with bone weakening, as overall the absolute loss of cortical bone would be rather small. Therefore this dimensional aspect at this specific site may bias the measure of cortical porosity and lead to its underestimation. To avoid such a potential bias, some investigators restrained its assessment to a sub-region where cortical bone is the thickest, i.e. the 40 most proximal slices (23).

Nevertheless, given its important role in load transfer and for consolidating the cancellous bone compartment, it is well possible that even such a small loss of bone mass could lead to drastic reduction in bone mechanical integrity, hence the importance to account for cortical porosity in bone strength prediction.

The purpose of the present study was to define the role of cortical porosity in *in vivo* bone strength assessment. Our hypothesis was that cortical porosity can predict bone strength, along with other microarchitectural features. To do so, we used HR-pQCT scans from the OFELY study to investigate the microarchitectural changes in both the trabecular and cortical compartments, as they occur with age, and bone strength as determined by micro finite element (µFE) analyses.

MATERIAL AND METHODS

Subjects

All subjects were participants of the Os des Femmes de Lyon (OFELY) population-based cohort, a prospective study of the determinants of bone loss in 1039 volunteer women recruited between February 1992 and December 1993. Those women were randomly selected from the affiliates of a large health insurance company (Mutuelle Générale de l'Education Nationale) from the Rhône district, i.e. Lyon and its surroundings in France (24, 25). All women recruited in the cohort were Caucasian. Between 2005 and 2007, 688 women came for their 14th visit (age from 44 to 95 years old). During this period 168 young women, aged 25 to 42 years old, were recruited in order to complete our cohort for young women data. In total, 857 women came for this visit. The protocol was approved by an Independent Ethics Committee and all patients gave written informed consent prior to participation. The OFELY cohort has been described in detail elsewhere (24, 25).

Measurement of bone mineral density and bone microarchitecture

Ultradistal radius and total hip areal bone mineral densities (aBMD, g/cm^2) were measured using dual-energy X-ray absorptiometry (DXA, QDR-A 4500, Hologic, Bedford, MA, USA). Volumetric bone mineral densities and microarchitecture were measured at the distal radius and tibia using a HR-pQCT device (XtremeCT, Scanco Medical AG, Brüttisellen, Switzerland) that acquires a stack of 110 parallel CT slices with an isotropic voxel size of 82 µm with a matrix size of 1536 × 1536. All scans have been performed according to the standard scan protocols: nominal high voltage of 60 kVp, X-ray tube current of 900 µA, for total scan time of 2.8 min and an effective dose lower than 3µSv per scan (26, 27). Despite the immobilization setup in carbon cast during the examination, motion artifacts could be observed on a single slice preview displayed at the end of each scan. As recommended by the manufacturer and with the agreement of the participant, scans could be repeated up to 3 times in order to improve the image quality.

Methods used to process the CT data have been previously described in detail by Laib and colleagues (26). Briefly, the entire volume of interest was segmented using a Laplace-Hamming filtering process

which aim was to enhance edge detection of trabecular structure. The choice of this segmentation method was justified by the non-negligible amount of partial volume effects that does not allow an optimal segmentation at this resolution when using a simple threshold method. The outcome variables were found to be highly correlated with µCT measurements at 28 µm resolution (28, 29).

Non-dominant limbs were always measured by DXA or HR-pQCT, unless it sustained fracture in the past in which case the contralateral limb was measured. Daily quality control phantom were performed to check for possible drifts in the X-ray sources. HR-pQCT quality scans were reviewed by an experienced operator on fully reconstructed scans, and graded into 5 classes from 0 for perfect scans to 4 for the poorest scans as described elsewhere (30). Scans with poor quality, i.e. grade 4, were excluded from the analyses.

An established semi-automatic segmentation script was used to differentiate cortical bone from trabecular bone (13-15), which permitted to measure cortical thickness using a direct transformation method. This method also permitted the assessment of cortical porosity which is not available in the standard microarchitecture evaluation.

The bone morphology parameters used in our analyses were averaged over the complete bone volume, i.e. the 110 slices. We assessed total, cortical and trabecular bone cross-sectional area (Tt.Ar, Ct.Ar and Tb.Ar, mm^2), volumetric bone density for total, cortical and trabecular bone (Tt.vBMD, Ct.vBMD and Tb.vBMD, mg/cm^3); cortical thickness (Ct.Th, µm) and porosity (Ct.Po, %); trabecular number (Tb.N, mm^{-1}), and intra-individual distribution of trabecular separation (Tb.Sp.SD, µm) in the refined compartments (26). Non metric trabecular indices were also assessed: the structural model index (SMI, no unit) related to the rod- or plate-like topology of the trabecular network, and the connectivity density (Conn.D, no unit).

Finite Element Analysis

Finite element models of the radius and the tibia were created directly from the segmented HR-pQCT images using software delivered with the HR-pQCT device (IPL, Scanco Medical AG). Cortical and trabecular bone were separated as described above for the microarchitecture assessment (13). The µFE simulation for the radius bone was already described in detail earlier (8). Briefly, a voxel-conversion

procedure was used to convert each voxel of bone tissue into an equally sized brick element (31), thus creating µFE models that represent the actual bone microarchitecture in detail. Material properties were chosen isotropic and elastic. Cortical and trabecular bone elements were assigned a Young's modulus of 20 and 17 GPa, respectively (32). All elements were assigned a Poisson's ratio of 0.3. A compression test was simulated in which a load in the longitudinal direction was applied at one end while the other end was fully constrained, to simulate a fall from standing height on the outstretched hand (33), representing the most common trauma associated with Colles fractures. The failure load was calculated using the criterion developed by Pistoia et. al which was modified to account for differences in material properties as described earlier (8, 34-37). The same parameters were used for the tibia analysis, as this was shown earlier to be associated with fragility fractures (9, 10).

In addition to failure load (N), µFEA derived variables used in our study included: stiffness (N/mm), the percentage of load carried by the trabecular bone at the distal and proximal surface of the volume of interest (Tb.Dist.Load and Tb.Prox.Load, in %), and the average and SD values of the Von Mises Stresses (VMS) in the trabecular and cortical bone (Tb.VMS and Ct.VMS; Tb.VMS.SD and Ct.VMS.SD, MPa) for a 1000 N applied load. All µFE analyses were done using the FE solver integrated in the IPL software v1.13 (Scanco Medical AG).

Statistical analysis

In this cross-sectional analysis examining the association between microarchitecture, bone mechanical properties and age, we have distinguished premenopausal and postmenopausal women. In most cases, the distribution of variables was not normal in each group even when log-transformed, thus all results were presented using the median and the interquartile range. Non-parametric Wilcoxon and Spearman tests were performed to assess respective differences between the two groups and the correlations between the variables. Linear regression with age as the predictor variable was performed in each menopause group, where correlation coefficients are noted r_{age}.

All data were summarized with respect to mean and SD of a sub-group of the premenopausal group, constituted of 65 healthy premenopausal women younger than 35 who never had any fragility fracture, did not report pregnancy or breast-feeding, or treatment intake, and were therefore used as the

reference group. This allowed us to transform all the data as T-scores, and to use standardized variables to build a multivariate stepwise descending regression analyses in order to find the microarchitectural determinants of bone strength. Stepwise descending linear regression models were computed in order to exclude parameters having negligible contributions to the variance of the final model predicting the failure load (R^2), i.e. when their respective semipartial correlation coefficient r^2 were lower than 0.02. Statistical analyses were performed using Stata software (v10.0).

RESULTS

We present descriptive characteristics of the cohort in Table 1, accounting for the menopausal status. There were 267 (31%) premenopausal women and 590 (69%) postmenopausal women, who all had at least either 1 valid radius scan or 1 valid tibia scan. A total of 11 radius and 9 tibia scans were excluded due to poor quality (grade 4), 1 radius and 2 tibia scans could not be performed due to patient insufficient mobility, 1 tibia scan could not be performed because of a technical issue during scanning, and 5 radius and 4 tibia scans could not be restored from the archive due to technical issues. Consequently, there were 834 radius scans and 841 tibia scans that could be used in this study. Three premenopausal women reported the use of bisphosphonates, hormone replacement therapy (HRT) or selective estrogen receptor modulator (SERM). Thirty percent of postmenopausal women, reported use of medication: 13.2% were taking bisphosphonates, 10% had HRT, 2.5% SERM, 2.2% antiaromatase inhibitors, 1.7% tibolone, and 0.3% had reported the use of glucocorticoids over 3 months.

Six hundred and ten women (71%) also had DXA measurements at the ultradistal radius. Valid proximal femur DXA measurements were obtained in 836 (97%) women.

Premenopausal women

Before the menopause, we observed a significant though moderate deterioration with age of microarchitectural parameters, as presented in Table 2. Precisely, until the menopause Ct.Po increased

from 0.71 to 1.02% at the radius resulting in a significant, though low, correlation with age (r_{age}=0.27, p<0.001). At the tibia, Ct.Po varied from 3.55 to 4.84%, also with a significant but low correlation with age (r_{age}=0.38, p<0.001). The SMI increased by 0.5% at the radius and 11% at the tibia, with correlations with age at r_{age}=0.15 and 0.28 respectively. Other microarchitectural parameters were also modestly correlated with age, with little variations until the onset of menopause. Among others Tb.N correlations to age were r_{age}=-0.22 and -0.05, respectively at the radius and the tibia, with a relative loss lower than 5% until the onset of menopause.

At the tibia particularly, we found a significant decrease of all vBMD measures and for the tibia bone stiffness with age. Tb.vBMD diminished significantly by 8.9% at the tibia through the premenopausal period (r_{age}=-0.21, p<0.001). The tibia stiffness decreased by 2.1% in the same period, but also had a low correlation with age (r_{age}=-0.12, p<0.001). At the radius, there was no significant variation with age for these parameters, although the failure load diminished by the same magnitude of 2.6% during this period. Also, we observed that at both sites, the amount of the total load carried by the trabecular bone compartment was less than 50%, and decreased significantly before the onset of menopause.

Postmenopausal women

After the onset of menopause, we observed steep decline with age of bone microarchitecture as illustrated in the plots in Figures 1 and 2. Detailed relation with age can be found for all parameters in Table 3, showing that most parameters had significant correlation with age, with $|r_{age}|$ values ranging from 0.10 up to 0.64.

Among all variables, it was cortical porosity that showed the largest variations with age: the absolute increase at the radius was from 1.53 to 3.28% (r_{age}=0.30, p<0.001), and at the tibia the increase with age was even stronger starting from 8.09% for women just entering the menopause until 23.48% for the oldest women (r_{age}=0.59, p<0.001), as illustrated in Figure 1A. It can be noted that Ct.Ar and SMI had stronger correlation with age at the radius, than at the tibia, as illustrated in Figures 1B and 1C. The degradation of bone microarchitecture translates into a weakening of bone that we observed with the significant decrease of failure load at the radius and tibia, with r_{age}=0.-44 and -0.42 respectively

(both $p<0.001$). Over the whole period of menopause, failure load diminished by 30% and 25%, at the radius and tibia respectively (Figure 2).

When compared to premenopausal women, almost all variables where significantly different, except the Tt.Ar, the Tb.Dist.Load and Tb.Prox.Load at the radius. For those parameters the relative differences between those two groups were less than 3%, when the difference ranged from 10% to 20% for other parameters of density, microarchitecture or biomechanics. Volumetric densities were significantly lower from -11 to -20% between pre- and postmenopausal women. For structural parameters, Ct.Th for example reduced by -14% at the radius and only by -6% at the tibia, when Tb.N declined by -11 and -9% at the radius and the tibia, respectively. Average Von Mises stresses in both cortical and trabecular bone increased from +16 to +24% between the two groups. A relative comparison of failure load between pre- and postmenopausal women showed a significant loss of bone strength of 20% at the radius and 15% at the tibia (both $p<0.001$).

Best predictors of Bone strength

To predict bone failure load in each menopausal status group, we chose to include anthropometric variables (age, height, and weight), geometric parameters (Ct.Ar and Tb.Ar) and all microarchitecture variables: Ct.Th, Ct.Po, Tb.N, Tb.Sp.SD, SMI and Conn.D into a multivariate model. At this stage all variables were transformed as T-score prior to including them in the multivariate model.

We first built our backward stepwise regression model on the whole population, where bone failure load was explained only by Ct.Ar, Tb.Ar, Ct.Po and SMI with total R^2 ranging from 0.90 to 0.95, independently of bone site or menopausal status. Other parameters were not significantly associated with failure load ($p>0.05$), or they had an insufficient contribution to explain failure load ($r^2<0.02$).

Results were also analysed separately for the premenopausal and postmenopausal group using the same model as for the whole population, as presented in Table 4. At the radius, in both groups, Ct.Ar and SMI explained most of the variance in the radius failure load ($R^2=0.90$). The Tb.Ar played a modest role in explaining failure load, with $r^2=0.058$ and 0.022 in premenopausal and postmenopausal women respectively. In premenopausal women, Ct.Po was not associated with bone strength, whereas

in the postmenopausal group, porosity became a significant predictor in the model (R^2=0.92), but bringing only a modest contribution (r^2=0.026).

At the tibia, in premenopausal women, the pattern of the multivariate regression was similar to the model obtained in postmenopausal women at the radius. Indeed Ct.Po brought a modest contribution (r^2=0.024), whereas the model was mostly held by the combination of Ct.Ar, Tb.Ar and SMI (R^2=0.95). In postmenopausal women, the 4-variable model was still highly predictive of the tibia failure load with R^2 = 0.94. However in this model, Ct.Po gained influence as its semipartial regression coefficient r^2 rose above that of Tb.Ar (r^2=0.218 vs 0.126, respectively). Also we noticed that the Ct.Ar semipartial correlation coefficient was no longer the most important contributor to the model as it was the case for the 3 previous models, and was smaller than that of the SMI (r^2=0.285 vs 0.352, respectively). All semipartial correlation coefficients for those 4 parameters were about the same magnitude in this very last model.

DISCUSSION

In this cross-sectional analysis, we found that cortical and trabecular properties, along with the failure load, deteriorated slightly with age in premenopausal women, whereas in postmenopausal women, cortical porosity and failure load were markedly deteriorated with age.

Recent HR-pQCT fracture studies – in this cohort or other cohorts – have shown that bone strength estimates were associated with prevalent fragility fracture in post-menopausal women, partly independently from DXA aBMD (6-12, 38). In this work, we showed that the radius bone failure load was stable before the onset of menopause, and decreased linearly with age afterwards. At the tibia, we observed the decline of bone strength even during the premenopausal period, with a steeper decline after the onset of menopause. Also, we have observed that the greatest relative loss were found for cortical bone parameters, in agreement with results reported in HR-pQCT studies conducted in other populations (16, 39). More importantly, we found that cortical porosity had a major role to play in failure load prediction in postmenopausal women, but only at the tibia, along with cortical and

trabecular areas, and the trabecular SMI. Although we observed the same exponential increase of cortical porosity with age at the radius, in contrast to what was suggested based on results of ex-vivo tests (15, 16) this has a very modest role in bone strength prediction at this site.

The role of cortical porosity in bone strength has already been addressed individually in type 2 diabetes mellitus (T2DM) patients (21, 40). Indeed this population has a high incidence of fractures, though the subjects generally have normal to high BMD compared to controls (21). The authors identified an increased cortical porosity in T2DM patients that could be the possible cause of the high fracture rate in this population. Also, a comparative µFE analysis where pores were or were not occluded showed that cortical porosity caused a loss of 2.5% and 5.8% of bone failure load, assessed respectively at the radius and the tibia. Interestingly those patients had higher volumetric BMD, despite the important cortical porosity, notably due to a thickening of the trabeculae in the outer part of the trabecular compartment. At the hip it has been shown that not only cortical thinning, but also cortical porosity increase was more pronounced in strategic regions of the femoral neck, particularly in fracture cases (17).

In order to better understand the relative impact of each microarchitectural feature on bone strength, we have conducted multivariate regression models to predict bone strength as assessed by µFE, in groups as a function of the subjects' menopausal status. Our hypothesis being that cortical porosity would be found as one of the predictors of bone failure load.

The general trend resulting from the analyses shows that bone failure load is mainly dependent on 4 variables: the cortical and trabecular areas, cortical porosity and the structural model index of trabecular bone. It is interesting to note that area parameters can be regarded as bone quantity parameters, as they represent the potential maximum amount of bone material. Cortical porosity and SMI come here as the respective microarchitectural features of each bone compartments, hence complementing bone strength prediction.

First when comparing the two variables of trabecular bone, the size of the trabecular compartment was never dominant as compared to the SMI, which confirms the importance of having a precise

understanding of the trabecular microarchitecture (27). This was emphasized at the radius site regardless of the menopausal status, where the trabecular area semipartial correlation coefficient indicated it played a modest role in the prediction of bone strength. On the other hand, when comparing cortical variables impact on the prediction model, cortical porosity had a substantial participation in bone strength prediction only at the tibia of postmenopausal women, as already outlined in type 2 diabetes mellitus (T2DM) studies (21, 40). Finally, cortical area was the most important variable to predict bone strength in 3 out of our 4 models. It is only at the distal tibia in postmenopausal women where it fell behind the SMI where it strengthens the role of SMI, and generally of trabecular bone microarchitecture in the prediction of bone strength, as outlined previously.

In premenopausal women, at both the radius and tibia, our multivariate regression of failure load showed that cortical porosity played a modest role. This could be explained by the very low amount of porosity. Our statistical model also revealed that cortical porosity was a poor predictor of bone strength at the radius. Despite the fact that cortical porosity followed an exponential law, as also observed in other populations (16, 39), in postmenopausal women its level barely rose above 4% at the radius, whereas it went beyond 10% at the tibia. It is also surprising because the tibia benefits from the mechanical stimulation which should help to protect it from bone loss. Technical issues may explain this low level of porosity at the radius. It may be partially due to the high variability of cortical thickness measures at the radius (22). It is indeed very thin on its distal half, when it becomes thick starting from the middle of the scan until its proximal end (21, 22). In addition, even in spectacular cases of high cortical porosity at the radius, such as in T2DM, cortical porosity seemed to be concentrated on the proximal half of the scan (21).

At the distal end of the radius scans, we could not evaluate void spaces smaller than 82µm and hence maybe led us to underestimate them. Based only on our results, we should only state that there seems to be a threshold for cortical porosity that cannot be achieved at this scanned site to consider it a major predictor of bone strength. Women in their 50s in our cohort had a cortical porosity level of 8%, which

can be suggested as the threshold level as measured by HR-pQCT when it gains weight in the failure load prediction.

There are several limitations to this study. First it is a cross-sectional analysis, thus the evolution observed with age among all our women may differ from the real intra-individual bone loss with aging. Moreover, HR-pQCT technical limitations should not be ignored. As already discussed its resolution of 82µm not only does not permit an accurate depiction of the trabecular number or SMI (41), but also underestimates cortical porosity even if those measurements were highly correlated to measurements obtained from µCT scans on ex vivo pieces (14, 29). Also refined depiction of the trabecular network into rod and plates might improve our multivariate model in further studies (42, 43). Second, it was reported that scan quality affected the reproducibility of measurements of fine structure such as the trabecular number, even for a drop in quality from grade 0 to 1 (30, 44). We can expect the same issue with the assessment of cortical porosity. In a recent study, the short term reproducibility of cortical porosity measurements was found to be only around 10% for the distal radius and 8% for the tibia (45). In that study it was shown that 3D registration would reduce this reproducibility error for cortical porosity, but not for most other measures, but has the disadvantage of further reducing the volume of interest in particular at the cortex. Third, our µFE model was a uniaxial compression model assuming homogeneous and isotropic material properties for each bone voxel, and simulating the main loading that occurs during a Colles' fracture during a fall on the outstretched hand. However, this is not the only situation where Colles' fracture occurs as observed recently (46). In that study, fractured women were asked to describe the situation of fall during which they had their wrist fractured: only 27 women out of 100 fell forward on their outstretched hand. Although independent of the fall type, the compressive component will be the major loading mode, it is possible that in these other cases also some bending and torsion loading will play a role. It can be added that this µFE model ignores the sources of fragility arising from the tissue level, e.g. from the quality of cross links (47), or the density of microdamages (18, 48). While the mineral apatite acts on stiffness, the organic matrix is primarily responsible for the post-yield and creep behaviour of bone and for its toughness (49). However, this is difficult to quantify and likely to vary across bone sites, therefore to

be different at the distal radius and tibia. Finally, our study showed the importance of cortical porosity only at the ultradistal tibia, which is not a common fragility fracture site. Nonetheless the added value of those data comes from the cortical nature of the skeleton in general, and it might be relevant to extrapolate those results for the femoral neck bone quality.

The main strength of this study came from the population studied. The OFELY cohort is a monocentric study of exclusively Caucasian women as described since the beginning of the follow up in 1992 (24, 25). There was no restrictive criterion regarding patient inclusion, making this population representative of the French women population. Therefore the variability induced by diseases or ethnical differences was reduced.

In conclusion, in our large cohort of French women, we observed a decline of bone strength at the tibia before the onset of menopause. The decline in failure load was more marked after the menopause and could be predicted by the combination of cortical and trabecular areas, cortical porosity and SMI. Despite a great deal of interest in new techniques to assess cortical bone, the influence of cortical porosity seemed to be sizeable compared with other parameters only at the distal tibia.

ACKNOWLEDGEMENTS

We thank A. Bourgeaud-Lignot, B. Vey-Marty and W. Wirane for valuable technical assistance. This study was supported in part by the ECTS/Servier Fellowship granted in 2009 to Nicolas Vilayphiou.

Index of tables

Index of figures

Table 1: General characteristics and DXA data of pre- and postmenopausal women, presented as median [IQR] (* $p<0.01$).

	Premenopausal women (n=267)	**Postmenopausal women (n=590)**
Variable	Median [IQR]	Median [IQR]
Age [yrs]	42 [35 ; 48]	68* [65 ; 73]
Height [m]	1.63 [1.59 ; 1.67]	1.59* [1.55 ; 1.62]
Weight [kg]	60 [54 ; 67]	619 [55 ; 68]
UDR.aBMD [g.HA/cm²]	0.420 [0.394 ; 0.461]	0.354* [0.313 ; 0.402]
THip.aBMD [g.HA/cm²]	0.947 [0.885 ; 1.024]	0.836* [0.751 ; 0.916]
Fractures (n)	1	116
Treatments (n)	3	177

Table 2: Microarchitecture and biomechanical results in premenopausal women at the radius and the tibia, presented as median [IQR] (* p<0.01)

	Radius (n=260)		Tibia (n=263)	
Variable	**Median [IQR]**	**r_{age}**	**Median [IQR]**	**r_{age}**
Tt.Ar [mm²]	253 [227 ; 277]	0.03	627 [552 ; 703]	0.09
Ct.Ar [mm²]	48 [42 ; 53]	0.16*	105 [96 ; 114]	0.11
Tb.Ar [mm²]	196 [171 ; 221]	-0.01	512 [439 ; 587]	0.08
Tt.vBMD [mgHA/cm³]	327 [291 ; 371]	0.06	307 [272 ; 347]	-0.15*
Ct.vBMD [mgHA/cm³]	900 [875 ; 928]	0.12	913 [876 ; 939]	-0.16*
Tb.vBMD [mgHA/cm³]	164 [144 ; 191]	-0.04	167 [144 ; 198]	-0.21*
Ct.Th [mm]	0.897 [0.805 ; 1.01]	0.10	1.181 [1.059 ; 1.331]	0.05
Ct.Po [%]	0.155 [0.147 ; 0.167]	0.28*	0.17 [0.154 ; 0.189]	0.21*
Tb.N [1/mm]	1.72 [1.58 ; 1.88]	-0.22*	1.61 [1.47 ; 1.81]	-0.05
Tb.Sp.SD [mm]	0.225 [0.188 ; 0.279]	0.30*	0.24 [0.21 ; 0.28]	0.15*
SMI	2.09 [1.85 ; 2.31]	0.15*	1.74 [1.44 ; 1.97]	0.28*
Conn.D	3.23 [2.72 ; 3.72]	-0.05	2.93 [2.39 ; 3.53]	0.00
Tb.Dist.Load [%]	42 [37 ; 48]	-0.14*	44 [40 ; 50]	-0.15*
Tb.Prox.Load [%]	13 [10 ; 17]	-0.16*	25 [21 ; 30]	-0.16*
Tb.VMS [MPa]	6.8 [6.1 ; 7.4]	-0.16*	3 [2.7 ; 3.2]	-0.06
Tb.VMS.SD [MPa]	4.3 [3.8 ; 4.8]	0.03	1.6 [1.4 ; 1.8]	0.18*
Ct.VMS [MPa]	13.5 [12.2 ; 14.9]	-0.01	5.5 [4.9 ; 6.2]	0.11
Ct.VMS.SD [MPa]	3.1 [2.7 ; 3.6]	0.12	0.9 [0.8 ; 1]	0.25*
Stiffness [N/mm]	142740 [127730 ; 160580]	0.00	381680 [340030 ; 422980]	-0.12*
Failure Load [N]	3374 [3021 ; 3800]	0.01	9023 [8024 ; 9971]	-0.11

Table 3: Microarchitecture and biomechanical results in postmenopausal women at the radius and the tibia, presented as median [IQR] (* p<0.01)

	Radius (n=571)		Tibia (n=578)	
Variable	**Median [IQR]**	**r_{age}**	**Median [IQR]**	**r_{age}**
Tt.Ar [mm²]	253 [226 ; 282]	0.02	**664 [590 ; 733]**	0.07
Ct.Ar [mm²]	**41 [35 ; 47]**	-0.42*	**99 [87 ; 109]**	-0.44*
Tb.Ar [mm²]	**203 [176 ; 232]**	0.10*	**551 [480 ; 625]**	0.10*
Tt.vBMD [mgHA/cm³]	**270 [221 ; 317]**	-0.44*	**251 [213 ; 283]**	-0.40*
Ct.vBMD [mgHA/cm³]	**800 [741 ; 855]**	-0.55*	**743 [668 ; 811]**	-0.64*
Tb.vBMD [mgHA/cm³]	**139 [108 ; 168]**	-0.34*	**147 [121 ; 173]**	-0.20*
Ct.Th [mm]	**0.77 [0.665 ; 0.895]**	-0.39*	**1.111 [0.984 ; 1.257]**	-0.09*
Ct.Po [%]	**0.184 [0.164 ; 0.211]**	0.17*	**0.213 [0.19 ; 0.236]**	0.37*
Tb.N [1/mm]	**1.57 [1.33 ; 1.77]**	-0.37*	**1.51 [1.32 ; 1.72]**	-0.21*
Tb.Sp.SD [mm]	**0.275 [0.225 ; 0.369]**	0.38*	**0.28 [0.23 ; 0.34]**	0.18*
SMI	**2.26 [2.03 ; 2.51]**	0.24*	**1.84 [1.58 ; 2.08]**	0.08
Conn.D	**2.66 [1.99 ; 3.28]**	-0.35*	**2.65 [2.17 ; 3.23]**	-0.19*
Tb.Dist.Load [%]	43 [38 ; 48]	0.02	**49 [43 ; 55]**	0.25*
Tb.Prox.Load [%]	14 [10 ; 18]	0.13*	**28 [23 ; 33]**	0.21*
Tb.VMS [MPa]	**7.7 [7 ; 8.8]**	0.48*	**3.4 [3.1 ; 3.8]**	0.47*
Tb.VMS.SD [MPa]	**5.4 [4.6 ; 6.5]**	0.48*	**1.9 [1.6 ; 2.2]**	0.40*
Ct.VMS [MPa]	**16.4 [14.3 ; 18.9]**	0.46*	**6.3 [5.6 ; 7.1]**	0.35*
Ct.VMS.SD [MPa]	**4.2 [3.5 ; 5.1]**	0.45*	**1.3 [1.1 ; 1.5]**	0.54*
Stiffness [N/mm]	**114690 [96986 ; 132040]**	-0.46*	**320255 [279430 ; 360830]**	-0.41*
Failure Load [N]	**2697 [2307 ; 3091]**	-0.44*	**7625 [6726 ; 8520]**	-0.42*

Median values in bold fonts, indicates significant differences when compared to the premenopausal group.

Table 4: Stepwise descending regression analyses for bone strength prediction, in pre- and postmenopausal women at the radius and at the tibia

Radius Failure Load				**Tibia Failure Load**			
Premenopausal women		n=260		**Premenopausal women**		n=263	
Complete model		R^2=0.90		Complete model		R^2=0.95	
Variable	semipartial r^2	p	beta	Variable	semipartial r^2	p	beta
Ct.Ar	0.530	0.000	0.747	Ct.Ar	0.377	0.000	0.633
Tb.Ar	0.058	0.000	0.258	Tb.Ar	0.184	0.000	0.466
Ct.Po	*0.002*	*0.017*	*-0.048*	Ct.Po	0.024	0.000	-0.168
SMI	0.284	0.000	-0.554	SMI	0.284	0.000	-0.553
Postmenopausal women		n=569		**Postmenopausal women**		n=578	
Complete model		R^2=0.92		Complete model		R^2=0.94	
Variable	semipartial r^2	p	beta	Variable	semipartial r^2	p	beta
Ct.Ar	0.381	0.000	0.671	Ct.Ar	0.287	0.000	0.564
Tb.Ar	0.023	0.000	0.155	Tb.Ar	0.126	0.000	0.387
Ct.Po	0.026	0.000	-0.163	Ct.Po	0.219	0.000	-0.487
SMI	0.225	0.000	-0.513	SMI	0.358	0.000	-0.618

Figure 1: Evolution with age at the radius, and the tibia, for cortical porosity Ct.Po (A), cortical area Ct.Ar (B), and structural model index SMI (C). The solid lines represent the fitted mean from regression models.

Radius

Tibia

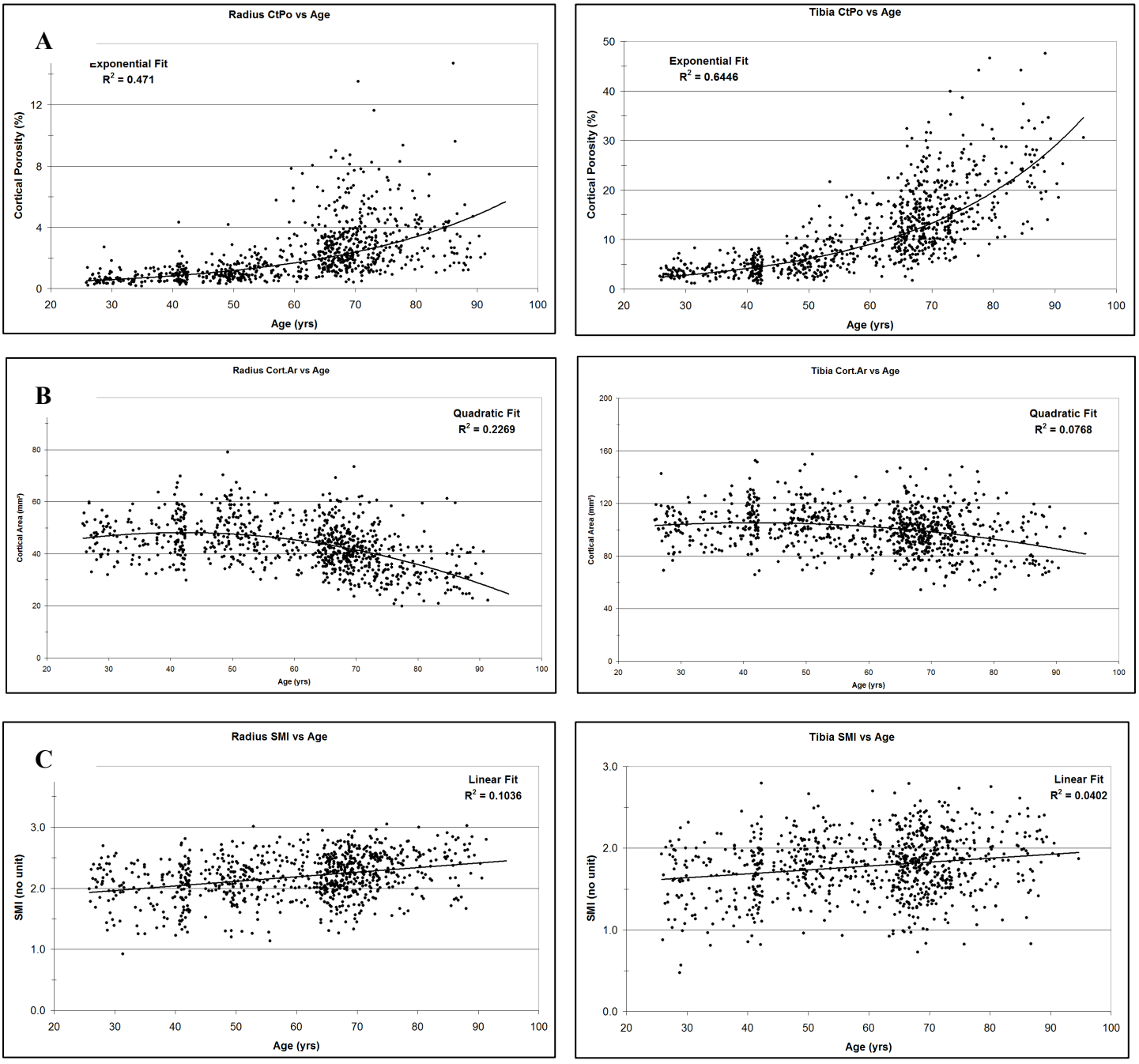

Figure 2: Evolution with age of Failure Load at the radius (A) and the tibia (B). The solid lines represent the fitted mean from regression models.

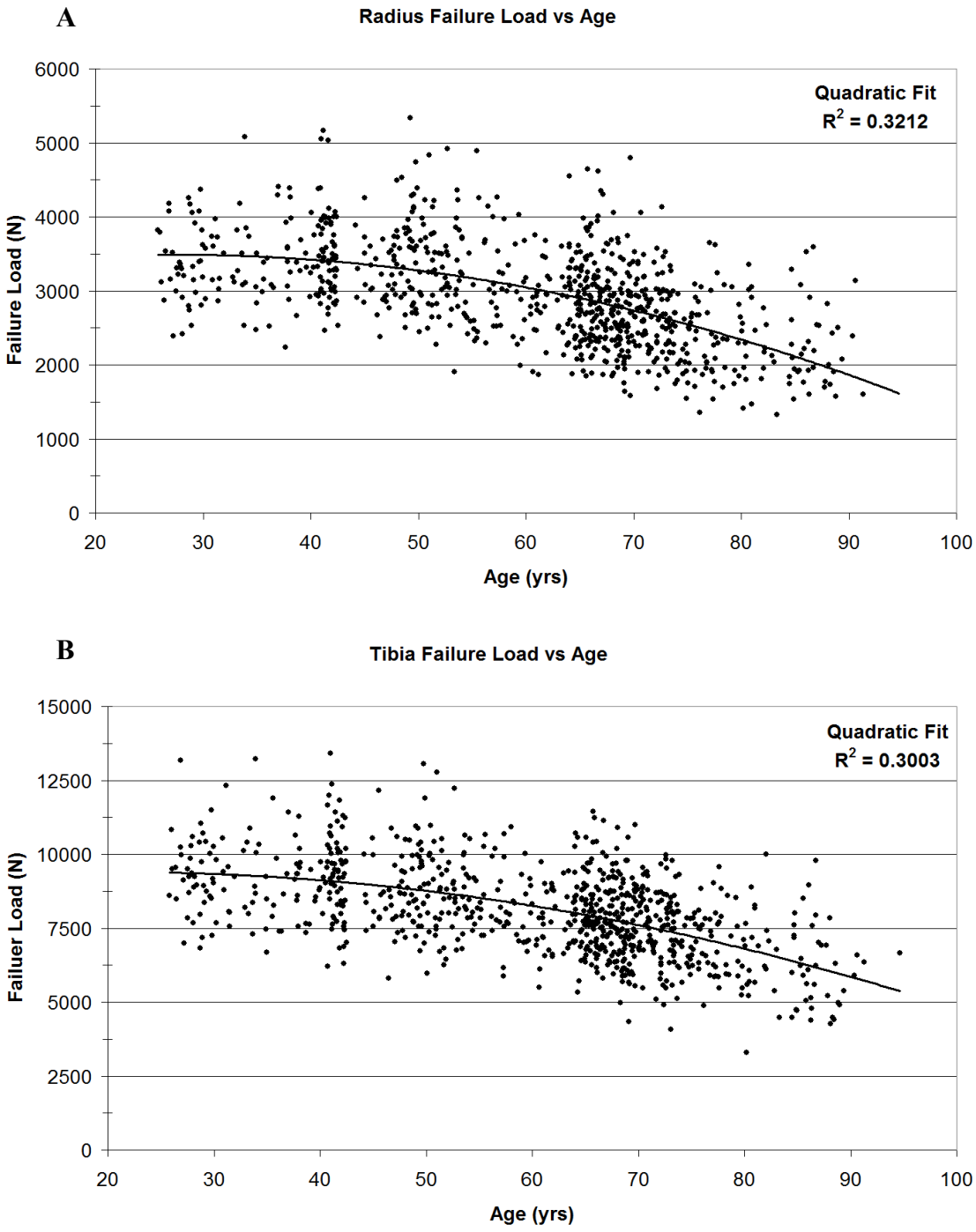

1. Anonymous Osteoporosis prevention, diagnosis, and therapy. NIH Consens Statement 17:1-45; 2000.
2. Schuit, S. C., van der Klift, M., Weel, A. E., de Laet, C. E., Burger, H., Seeman, E., Hofman, A., Uitterlinden, A. G., van Leeuwen, J. P., and Pols, H. A. Fracture incidence and association with bone mineral density in elderly men and women: the Rotterdam Study. Bone 34:195-202; 2004.
3. Siris, E. S., Chen, Y. T., Abbott, T. A., Barrett-Connor, E., Miller, P. D., Wehren, L. E., and Berger, M. L. Bone mineral density thresholds for pharmacological intervention to prevent fractures. Arch Intern Med 164:1108-12; 2004.
4. Sornay-Rendu, E., Munoz, F., Garnero, P., Duboeuf, F., and Delmas, P. D. Identification of osteopenic women at high risk of fracture: the OFELY study. J Bone Miner Res 20:1813-9; 2005.
5. Keaveny, T. M., and Bouxsein, M. L. Theoretical implications of the biomechanical fracture threshold. J Bone Miner Res 23:1541-7; 2008.
6. Melton, L. J., 3rd, Riggs, B. L., van Lenthe, G. H., Achenbach, S. J., Muller, R., Bouxsein, M. L., Amin, S., Atkinson, E. J., and Khosla, S. Contribution of in vivo structural measurements and load/strength ratios to the determination of forearm fracture risk in postmenopausal women. J Bone Miner Res 22:1442-8; 2007.
7. Melton, L. J., 3rd, Riggs, B. L., Keaveny, T. M., Achenbach, S. J., Hoffmann, P. F., Camp, J. J., Rouleau, P. A., Bouxsein, M. L., Amin, S., Atkinson, E. J., Robb, R. A., and Khosla, S. Structural determinants of vertebral fracture risk. J Bone Miner Res 22:1885-92; 2007.
8. Boutroy, S., Van Rietbergen, B., Sornay-Rendu, E., Munoz, F., Bouxsein, M. L., and Delmas, P. D. Finite element analysis based on in vivo HR-pQCT images of the distal radius is associated with wrist fracture in postmenopausal women. J Bone Miner Res 23:392-9; 2008.
9. Vilayphiou, N., Boutroy, S., Szulc, P., Van Rietbergen, B., Munoz, F., Delmas, P. D., and Chapurlat, R. Finite element analysis performed on radius and tibia HR-pQCT images and fragility fractures at all sites in men. J Bone Miner Res; 2010.
10. Vilayphiou, N., Boutroy, S., Szulc, P., van Rietbergen, B., Munoz, F., Delmas, P. D., and Chapurlat, R. Finite element analysis performed on radius and tibia HR-pQCT images and fragility fractures at all sites in men. J Bone Miner Res 26:965-73; 2011.
11. Stein, E. M., Liu, X. S., Nickolas, T. L., Cohen, A., Thomas, V., McMahon, D. J., Zhang, C., Yin, P. T., Cosman, F., Nieves, J., Guo, X. E., and Shane, E. Abnormal microarchitecture and reduced stiffness at the radius and tibia in postmenopausal women with fractures. J Bone Miner Res 25:2572-81; 2011.
12. Sornay-Rendu, E., Cabrera-Bravo, J. L., Boutroy, S., Munoz, F., and Delmas, P. D. Severity of vertebral fractures is associated with alterations of cortical architecture in postmenopausal women. J Bone Miner Res 24:737-43; 2009.
13. Burghardt, A. J., Buie, H. R., Laib, A., Majumdar, S., and Boyd, S. K. Reproducibility of direct quantitative measures of cortical bone microarchitecture of the distal radius and tibia by HR-pQCT. Bone 47:519-28; 2010.
14. Nishiyama, K. K., Macdonald, H. M., Buie, H. R., Hanley, D. A., and Boyd, S. K. Postmenopausal women with osteopenia have higher cortical porosity and thinner cortices at the distal radius and tibia than women with normal aBMD: an in vivo HR-pQCT study. J Bone Miner Res 25:882-90; 2010.
15. Buie, H. R., Campbell, G. M., Klinck, R. J., MacNeil, J. A., and Boyd, S. K. Automatic segmentation of cortical and trabecular compartments based on a dual threshold technique for in vivo micro-CT bone analysis. Bone 41:505-15; 2007.

16. Macdonald, H. M., Nishiyama, K. K., Kang, J., Hanley, D. A., and Boyd, S. K. Age-related patterns of trabecular and cortical bone loss differ between sexes and skeletal sites: a population-based HR-pQCT study. J Bone Miner Res 26*:*50-62; 2011.
17. Bell, K. L., Loveridge, N., Power, J., Garrahan, N., Meggitt, B. F., and Reeve, J. Regional differences in cortical porosity in the fractured femoral neck. Bone 24*:*57-64; 1999.
18. Diab, T., and Vashishth, D. Effects of damage morphology on cortical bone fragility. Bone 37*:*96-102; 2005.
19. Martin, R. B., and Burr, D. B. The microscopic structure of bone. Structure, function and adaptation of compact bone; 1989.
20. Zebaze, R. M., Ghasem-Zadeh, A., Bohte, A., Iuliano-Burns, S., Mirams, M., Price, R. I., Mackie, E. J., and Seeman, E. Intracortical remodelling and porosity in the distal radius and post-mortem femurs of women: a cross-sectional study. Lancet 375*:*1729-36; 2010.
21. Burghardt, A. J., Issever, A. S., Schwartz, A. V., Davis, K. A., Masharani, U., Majumdar, S., and Link, T. M. High-resolution peripheral quantitative computed tomographic imaging of cortical and trabecular bone microarchitecture in patients with type 2 diabetes mellitus. J Clin Endocrinol Metab 95*:*5045-55; 2010.
22. Boyd, S. K. Site-specific variation of bone micro-architecture in the distal radius and tibia. J Clin Densitom 11*:*424-30; 2008.
23. Zebaze, R., Ghasem-Zadeh, A., Mbala, A., and Seeman, E. A new method of segmentation of compact-appearing, transitional and trabecular compartments and quantification of cortical porosity from high resolution peripheral quantitative computed tomographic images. Bone 54*:*8-20; 2013.
24. Garnero, P., Borel, O., Sornay-Rendu, E., Arlot, M. E., and Delmas, P. D. Vitamin D receptor gene polymorphisms are not related to bone turnover, rate of bone loss, and bone mass in postmenopausal women: the OFELY Study. J Bone Miner Res 11*:*827-34; 1996.
25. Arlot, M. E., Sornay-Rendu, E., Garnero, P., Vey-Marty, B., and Delmas, P. D. Apparent pre- and postmenopausal bone loss evaluated by DXA at different skeletal sites in women: the OFELY cohort. J Bone Miner Res 12*:*683-90; 1997.
26. Laib, A., Hauselmann, H. J., and Ruegsegger, P. In vivo high resolution 3D-QCT of the human forearm. Technol Health Care 6*:*329-37; 1998.
27. Boutroy, S., Bouxsein, M. L., Munoz, F., and Delmas, P. D. In vivo assessment of trabecular bone microarchitecture by high-resolution peripheral quantitative computed tomography. J Clin Endocrinol Metab 90*:*6508-15; 2005.
28. Laib, A., and Ruegsegger, P. Calibration of trabecular bone structure measurements of in vivo three-dimensional peripheral quantitative computed tomography with 28-microm-resolution microcomputed tomography. Bone 24*:*35-9; 1999.
29. MacNeil, J. A., and Boyd, S. K. Accuracy of high-resolution peripheral quantitative computed tomography for measurement of bone quality. Med Eng Phys 29*:*1096-105; 2007.
30. Sode, M., Burghardt, A. J., Pialat, J. B., Link, T. M., and Majumdar, S. Quantitative characterization of subject motion in HR-pQCT images of the distal radius and tibia. Bone 48*:*1291-7; 2011.
31. van Rietbergen, B., Weinans, H., Huiskes, R., and Odgaard, A. A new method to determine trabecular bone elastic properties and loading using micromechanical finite-element models. J Biomech 28*:*69-81; 1995.

32. Turner, C. H., Rho, J., Takano, Y., Tsui, T. Y., and Pharr, G. M. The elastic properties of trabecular and cortical bone tissues are similar: results from two microscopic measurement techniques. J Biomech 32*:*437-41; 1999.
33. Chiu, J., and Robinovitch, S. N. Prediction of upper extremity impact forces during falls on the outstretched hand. J Biomech 31*:*1169-76; 1998.
34. Pistoia, W., van Rietbergen, B., Lochmuller, E. M., Lill, C. A., Eckstein, F., and Ruegsegger, P. Estimation of distal radius failure load with micro-finite element analysis models based on three-dimensional peripheral quantitative computed tomography images. Bone 30*:*842-8; 2002.
35. Macneil, J. A., and Boyd, S. K. Bone strength at the distal radius can be estimated from high-resolution peripheral quantitative computed tomography and the finite element method. Bone 42*:*1203-13; 2008.
36. Varga, P., Baumbach, S., Pahr, D., and Zysset, P. K. Validation of an anatomy specific finite element model of Colles' fracture. J Biomech 42*:*1726-31; 2009.
37. Mueller, T. L., Christen, D., Sandercott, S., Boyd, S. K., van Rietbergen, B., Eckstein, F., Lochmuller, E. M., Muller, R., and van Lenthe, G. H. Computational finite element bone mechanics accurately predicts mechanical competence in the human radius of an elderly population. Bone 48*:*1232-8; 2011.
38. Vico, L., Zouch, M., Amirouche, A., Frere, D., Laroche, N., Koller, B., Laib, A., Thomas, T., and Alexandre, C. High-resolution pQCT analysis at the distal radius and tibia discriminates patients with recent wrist and femoral neck fractures. J Bone Miner Res 23*:*1741-50; 2008.
39. Dalzell, N., Kaptoge, S., Morris, N., Berthier, A., Koller, B., Braak, L., van Rietbergen, B., and Reeve, J. Bone micro-architecture and determinants of strength in the radius and tibia: age-related changes in a population-based study of normal adults measured with high-resolution pQCT. Osteoporos Int 20*:*1683-94; 2009.
40. Patsch, J. M., Burghardt, A. J., Yap, S. P., Baum, T., Schwartz, A. V., Joseph, G. B., and Link, T. M. Increased cortical porosity in type 2 diabetic postmenopausal women with fragility fractures. J Bone Miner Res 28*:*313-24; 2013.
41. Sode, M., Burghardt, A. J., Nissenson, R. A., and Majumdar, S. Resolution dependence of the non-metric trabecular structure indices. Bone 42*:*728-36; 2008.
42. Liu, X. S., Cohen, A., Shane, E., Stein, E., Rogers, H., Kokolus, S. L., Yin, P. T., McMahon, D. J., Lappe, J. M., Recker, R. R., and Guo, X. E. Individual trabeculae segmentation (ITS)-based morphological analysis of high-resolution peripheral quantitative computed tomography images detects abnormal trabecular plate and rod microarchitecture in premenopausal women with idiopathic osteoporosis. J Bone Miner Res 25*:*1496-505; 2010.
43. Pialat, J. B., Vilayphiou, N., Boutroy, S., Gouttenoire, P. J., Sornay-Rendu, E., Chapurlat, R., and Peyrin, F. Local topological analysis at the distal radius by HR-pQCT: Application to in vivo bone microarchitecture and fracture assessment in the OFELY study. Bone 51*:*362-8; 2012.
44. Pialat, J. B., Burghardt, A. J., Sode, M., Link, T. M., and Majumdar, S. Visual grading of motion induced image degradation in high resolution peripheral computed tomography: Impact of image quality on measures of bone density and micro-architecture. Bone; 2011.
45. Ellouz, R., Chapurlat, R., van Rietbergen, B., Christen, P., Pialat, J. B., and Boutroy, S. Challenges in longitudinal measurements with HR-pQCT: evaluation of a 3D registration method to improve bone microarchitecture and strength measurement reproducibility. Bone 63*:*147-57; 2014.

46. Melton, L. J., 3rd, Christen, D., Riggs, B. L., Achenbach, S. J., Muller, R., van Lenthe, G. H., Amin, S., Atkinson, E. J., and Khosla, S. Assessing forearm fracture risk in postmenopausal women. Osteoporos Int 21*:*1161-9; 2010.
47. Berteau, J. P., Gineyts, E., Pithioux, M., Baron, C., Boivin, G., Lasaygues, P., Chabrand, P., and Follet, H. Ratio between mature and immature enzymatic cross-links correlates with post-yield cortical bone behavior: An insight into greenstick fractures of the child fibula. Bone 79*:*190-195.
48. Chapurlat, R. D., Arlot, M., Burt-Pichat, B., Chavassieux, P., Roux, J. P., Portero-Muzy, N., and Delmas, P. D. Microcrack frequency and bone remodeling in postmenopausal osteoporotic women on long-term bisphosphonates: a bone biopsy study. J Bone Miner Res 22*:*1502-9; 2007.
49. Currey, J. D. Role of collagen and other organics in the mechanical properties of bone. Osteoporos Int 14 Suppl 5*:*S29-36; 2003.